

# *Lake surface temperature [in “State of the Climate in 2018”]*

Article

Published Version

Carrea, L. ORCID: <https://orcid.org/0000-0002-3280-2767>,  
Woolway, R. I. ORCID: <https://orcid.org/0000-0003-0498-7968>,  
Merchant, C. ORCID: <https://orcid.org/0000-0003-4687-9850>,  
Dokulil, M. T., de Eyto, E., DeGasperi, C. L., Korhonen, J.,  
Marszelewski, W., May, L., Paterson, A. M., Rusak, J. A.,  
Schladow, S. G., Schmid, M., Verburg, P., Watanabe, S. and  
Weyhenmeyer, G. A. (2019) Lake surface temperature [in  
“State of the Climate in 2018”]. *Bulletin of the American  
Meteorological Society*, 100 (9). pp. 13-14. ISSN 1520-0477  
doi: 10.1175/2019BAMSStateoftheClimate.1 Available at  
<https://centaur.reading.ac.uk/85967/>

It is advisable to refer to the publisher’s version if you intend to cite from the work. See [Guidance on citing](#).

Published version at: <https://www.ncdc.noaa.gov/bams/2018>

To link to this article DOI:

<http://dx.doi.org/10.1175/2019BAMSStateoftheClimate.1>

Publisher: American Meteorological Society

All outputs in CentAUR are protected by Intellectual Property Rights law, including copyright law. Copyright and IPR is retained by the creators or other copyright holders. Terms and conditions for use of this material are defined in

the [End User Agreement](#).

[www.reading.ac.uk/centaur](http://www.reading.ac.uk/centaur)

## **CentAUR**

Central Archive at the University of Reading

Reading's research outputs online

2) LAKE SURFACE TEMPERATURE—L. Carrea, R. I. Woolway, C. J. Merchant, M. T. Dokulil, E. de Eyto, C. L. DeGasperi, J. Korhonen, W. Marszelewski, L. May, A. M. Paterson, J. A. Rusak, S. G. Schladow, M. Schmid, P. Verburg, S. Watanabe, and G. A. Weyhenmeyer

The satellite-derived lake surface water temperature (LSWT) used for this analysis is spatially averaged per lake for a total of 923 of the 1000 GloboLakes sites (Politi et al. 2016) for which high-quality temperatures were available in 2018. Lake-wide average surface temperatures have been shown to provide a representative picture of LSWT responses to climate change (Woolway and Merchant 2018). This analysis follows previous studies (Schneider and Hook 2010; O’Reilly et al. 2015; Woolway and Merchant 2017) in determining warm-season averages for midlatitude lakes [July–September in the Northern Hemisphere (NH); January–March in the Southern Hemisphere] and whole-year averages for tropical lakes.

In 2018, the satellite-derived LSWT anomaly averaged over the target lakes ( $n = 923$ ) was  $+0.17^{\circ}\text{C}$  compared to the 1996–2016 average. Thus, 2018 temperatures continue the warming trend identified in previous analyses (Woolway et al. 2017, 2018) of about  $0.27 \pm 0.01^{\circ}\text{C decade}^{-1}$ , although anomalies were  $0.14^{\circ}\text{C}$  and  $0.43^{\circ}\text{C}$  cooler than those observed in 2017 and 2016, respectively. The anomalies for each lake are shown in Plate 2.1b where latitudes have been maintained and longitude shifted to avoid overlapping of lakes in the plot. The LSWT anomaly was positive for 60% of lakes and negative for 40%. About 62% of the lakes in the NH above  $23.5^{\circ}$  latitude have positive anomalies.

The regions where lakes have the largest positive anomalies were Europe and East Asia, while cooler lakes were observed in North America around Canada and warmer lakes around the continental United States. Figure 2.2 shows spatial maps for: (a) Europe ( $n = 127$ ); (b) Africa ( $n = 68$ ); (c) Canada ( $n = 245$ ); and (d) the Tibetan Plateau ( $n = 106$ ). Regionally

averaged LSWT calculated from the satellite data shows a warming tendency of  $+0.50 \pm 0.03^{\circ}\text{C decade}^{-1}$  in Europe,  $+0.30 \pm 0.04^{\circ}\text{C decade}^{-1}$  in Canada, and  $+0.22 \pm 0.02^{\circ}\text{C decade}^{-1}$  in the Tibetan Plateau (Fig. 2.3). In Africa, the tendency is more neutral. The behavior of LSWT for the Tibetan area in these data appears to be in agreement with Wan et al. (2017) when daytime LSWT for July–September are considered. The period July–September 2018 was the warmest for European lakes since 1995, consistent with strong positive July–September averaged surface air temperature (SAT) anomalies (Fig. 2.2), calculated from the GHCN v3 (250-km smoothing radius) data of the NASA GISS surface temperature analysis (Hansen et al. 2010; GISTEMP Team 2016). Lake temperature anomalies broadly track surface temperature (Section 2b1), although factors such as wind speed, humidity, insolation, and the thermal time constants of lakes contribute to variation within this broad pattern.

Overall, 94% ( $n = 29$ ) of lakes with in situ LSWT measurements had positive anomalies in 2018. Similar to the satellite data, in situ positive anomalies were observed in Europe. For example, the second largest

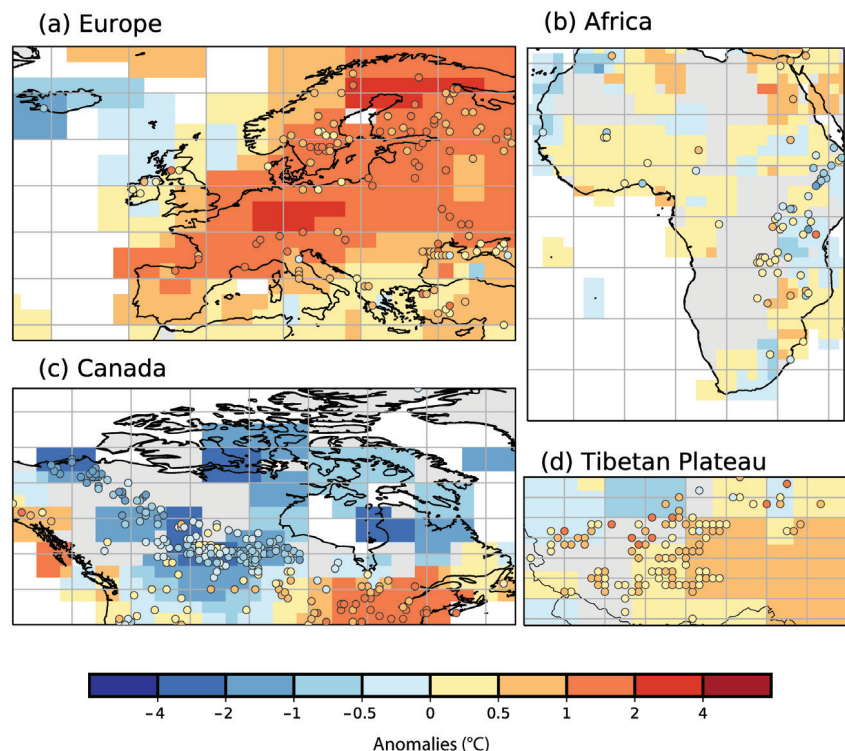


**FIG. 2.2. Satellite-derived lake surface water temperature anomalies in 2018. Shown are the patterns in lake temperature anomalies (colored points) together with surface air temperature (calculated from GHCN v3 data of the NASA GISS surface temperature analysis) (a) in Europe, (b) Africa, (c) Canada, and the (d) Tibetan Plateau. Air and lake surface water temperature anomalies ( $^{\circ}\text{C}$ ; relative to 1996–2016) are calculated for the warm season (Jul–Sep in NH; Jan–Mar in SH; and over the whole year in the tropics).**

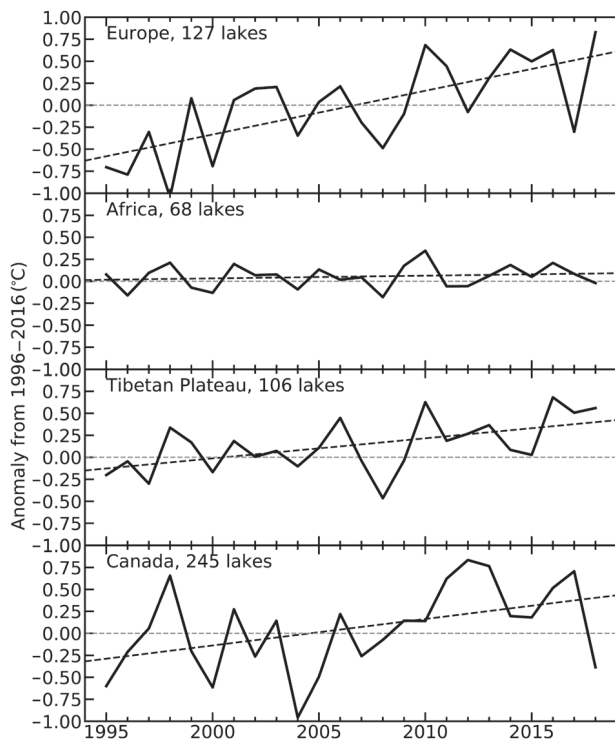


**FIG. 2.3. Satellite-derived annual lake surface water temperature anomalies from 1995 to 2018 for Europe, Africa, the Tibetan Plateau, and Canada. Shown are the regional average satellite-derived lake surface temperature anomalies. Annual lake surface water temperatures anomalies (°C; relative to 1996–2016) are calculated for the warm season (Jul–Sep in NH; Jan–Mar in SH; and over the whole year in the tropics).**

lake in Sweden by surface area, Vättern, had a LSWT anomaly of +2.1°C in 2018. A similar anomaly was observed in Lower Lake Zurich. The average 2018 LSWT anomaly for European lakes in the in situ collection was +1.2°C. Strong positive anomalies from in situ data were also observed in New Zealand lakes (+0.9°C).

Satellite and in situ observations consistently show strong positive anomalies across Europe, which is also confirmed by the global surface temperature analysis (Section 2b1) and the land surface temperature extreme (Section 2b3).

LSWT time series were derived from satellite observations from the series of Along Track Scanning Radiometers and the Advanced Very High Resolution Radiometers on MetOp A and B platforms, using the retrieval methods of MacCallum and Merchant (2012) on image pixels filled with water according to both the inland water dataset of Carrea et al. (2015) and a reflectance-based water detection scheme. LSWT from 1996 to 2016 have been derived with the GloboLakes project and the 2017–18 extension within

the Copernicus Climate Change Service (C3S) Programme. In addition, in situ lake surface temperature observations from some of the world’s best-studied lakes have been analyzed ( $n = 31$ ).

### 3) LAND SURFACE TEMPERATURE EXTREMES—A. D. King, M. G. Donat, and R. J. H. Dunn

As average temperatures have risen in most locations, there have been associated increases in warm extremes and reductions in the frequency and intensity of cold extremes. In 2018, the broad-scale pattern continued, with more widespread, frequent, and intense warm extremes coupled with fewer and less intense cold extremes.

The GHCNDEX dataset (Donat et al. 2013) is used for contextualizing temperature extremes in 2018. GHCNDEX uses the large archive of station data in the Global Historical Climatology Network - Daily (GHCND; Menne et al. 2012) known as Global Historical Climatology Network (GHCN) to calculate extreme indices proposed by the World Meteorological Organization Expert Team on Climate Change Detection and Indices (ETCCDI; Zhang et al. 2011). The format here follows that of previous *State of the Climate* reports. It should be noted that the available data are unfortunately sparse. The lack of spatial coverage is in part due to a lack of historical data in many areas of sub-Saharan Africa and northern South America (Donat et al. 2013) and in part because the 2018 data from some areas are incomplete at the time of writing due to delays from some data sources. As a result, many of the indices considered are restricted to North America, Europe, eastern Asia, and Australia (see Online Figs. S2.5–S2.7), but these observation-based anomalies are complemented with results from the ERA-Interim (Dee et al. 2011) and new ERA5 (Hersbach et al. 2019) reanalyses (see Online Figs. S2.8–S2.12). The indices considered here are shown in Table 2.2 and have been calculated both annually and seasonally with respect to a 1961–90 climatological base period.

In 2018, the annual anomalies of TX90p and TN10p indicate more frequent warm extremes and less frequent cool extremes compared to the climatological average for the majority of locations where data are available (Plates 2.1c,d). Across much of Europe, Australia, and the southwestern United States, there were around double the number of days where the daily maximum temperature was above the climatological 90th percentile than would be expected (36.5 by definition, Fig. 2.4). Continental Canada and a small area of northwest Africa are the only locations with available data that exhibited